International Journal of Microwave and Wireless Technologies

cambridge.org/mrf

A wideband and directive metasurface FPC antenna with toroidal metal structure loading

Parul Dawar[1] and Mahmoud A. Abdalla[2]

[1]Electronics and Communication Engineering Department, Guru Tegh Bahadur Institute of Technology, Delhi, India and [2]Electromagnetic Waves Group, Department of Electronic Engineering, Military Technical College, Cairo, Egypt

Research Paper

Cite this article: Dawar P, Abdalla MA (2022). A wideband and directive metasurface FPC antenna with toroidal metal structure loading. *International Journal of Microwave and Wireless Technologies* **14**, 1069–1080. https://doi.org/10.1017/S1759078721001380

Received: 15 June 2021
Revised: 6 September 2021
Accepted: 8 September 2021
First published online: 6 October 2021

Key words:
Front to back ratio; high directivity; metasurface; wideband

Author for correspondence:
Mahmoud A. Abdalla,
E-mail: maaabdalla@ieee.org

Abstract

In this paper, a novel metasurface-based Fabry–Perot cavity antenna loaded with toroidal metal structures is presented. The antenna is compact, wideband, and has high directivity and a high front-to-back ratio. The idea of the antenna is based on loading a microstrip narrow band patch antenna resonating at 4.5 GHz by a single layer metasurface superstrate and with a toroidal metal structure. The metasurface superstrate comprises a periodic array of square patch cells. Compared to conventional microstrip antenna, the front to back lobe ratio is increased from 7 to 20 dB and the directivity is increased by 7 dB. Also, the antenna impedance bandwidth is 34% which is increased four times. This is the first-ever antenna with enhanced bandwidth and directivity using a single layer of metasurface and that too made up of periodic cell array and has application as an energy harvester.

Introduction

Microstrip patch antenna has a low profile, low cost, small size, ease of fabrication. It can provide multi-operating frequencies, polarizations, and beam scanning functionality. Metamaterials are designed by patterning a set of small scatterers in an array yielding desirable bulk electromagnetic behavior. Various planar metamaterials were proposed for miniaturization and broad banding of antennas [1, 2]. However, improving the antenna efficiency and back lobe ratio remains challenging owing to lower bandwidth and higher loss of these antennas. Also, antennas for applications involving imaging at microwave frequencies should have higher directivity, broader bandwidth, and smaller size [3].

The problem of back lobe radiation and surface waves in microstrip antennas can be solved by backing the antennas with conductor reflectors or artificial magnetic conductors [4]. To increase the antenna directivity, one successful approach is using resonant cavity antenna (RCA) [5] where the antenna is loaded with partially reflecting artificial surfaces (PRS) as superstrates forming Fabry–Perot (FP) cavity [6].

The metasurface is a two-dimensional surface version of metamaterials that is obtained by arranging electrically small scatters/holes at a surface. Based on the pattern periodicity, the average tangential fields can be controlled using a local Floquet-wave expansion and hence, controlling the electromagnetic behavior at the surface [7]. Thanks to their unique electromagnetic manipulation, metasurface-based antennas are characterized with higher directivity, broader bandwidth, and smaller size than other planar antennas [8]. Metasurface structures have been further employed in developing FP cavity antennas with small RCS and high directivity [9].

Metamaterial resonators were based upon two basic shapes i.e. square and circle, forming labyrinth and circular split ring resonators (SRRs), respectively. It is observed that a high Q is attainable in toroidal shapes in such a way that the toroidal dipole radiation is neutralized by that of the electric dipole at a resonance frequency. It was well demonstrated resembling poloidal currents capable of inducing currents in SRRs and increasing, toroidal moment remarkably giving way for new extended scope in electrodynamics [10–12].

In this paper, a new design for the FPC antenna by loading a patch antenna, as a primary radiator, with a square patch-shaped 10×10 array as metasurface superstrate is presented. The novelty of the structure lies in the loading of a patch with a toroidal metal structure to achieve a wide band with a high front-to-back lobe ratio and directivity. The antenna contribution in the enhancement in bandwidth and directivity of the antenna over microstrip patch antenna with compact size. This enhancement is considered state-of-the-art as it is done using just a single layer of superstrate/reflective surface with toroidal metal structure. Moreover, it is useful as a capacitive energy harvester.

CAMBRIDGE UNIVERSITY PRESS

Metasurface FP cavity antenna

Fabry–Perot cavity antenna structure

The microstrip patch antenna is designed at 4.5 GHz on a substrate with dielectric constant $\varepsilon_r = 4.4$ and substrate thickness $H_S = 1.6$ mm. To construct a metasurface layer, square patches of 10×10 array of side $D_{HOLE} = 3.5$ mm are etched on a thin dielectric layer ($H << Hs$) in such a way that each cell is spaced by $Dx \times Dy = 3.5 \times 3.5$ mm^2. This metasurface layer is placed as a superstrate for the patch antenna at a distance $H_{MS} = 0.8$ mm above the patch. The dielectric medium between the patch and metasurface is air (ε_0) and between patch and ground plane is FR4 ($\varepsilon_r = 4.4$). The feeding transmission line dimensions were optimized to match the 50 Ω feeding port. The detailed metasurface-loaded antenna is shown in Fig. 1(a) for the top view, Fig. 1(b) for the side view, and Fig. 1(c) for the bottom view (the bottom view shows the ground plane as PEC).

The average tangential (transverse to z) field on it is given by (1) [13].

$$\begin{bmatrix} E \\ H \end{bmatrix} = \frac{1}{d^2} \iint_{-\frac{d}{2}}^{\frac{d}{2}} \begin{bmatrix} e \\ h \end{bmatrix} e^{jk.\rho} dx.dy \tag{1}$$

where E and H is tangential electric and magnetic field, d is periodicity, k is transverse wave vector, ρ is arbitrary observation point of the metasurface. Based on the phase reflection optimization properties of the metasurface the patch antenna radiation can be concentrated. In other words, it acts as a lens focusing on the EM radiations.

Fabry–Perot cavity design principles

The 3D geometry of the FPC antenna is shown in Fig. 2. In the design of the reflective structure, the attention was focused on the directive gain improvement and bandwidth enhancement simultaneously. The gain and fractional bandwidth are functions of the reflection coefficient in FP cavity are given by (2) and (3) [14, 15]:

$$G = \frac{1+R}{1-R} \tag{2}$$

$$FBW = \frac{\Delta f}{f_0} = \frac{\lambda}{2\pi L_r} \times \frac{1-R}{\sqrt{R}} \tag{3}$$

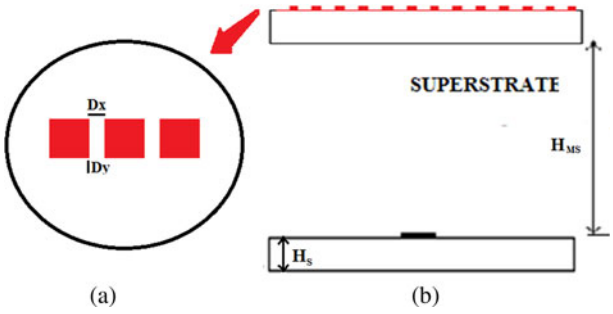

Fig. 2. Fabry–Perot cavity:(a) enlarged view of the unit cell of superstrate (b) patch antenna with superstrate.

where G is gain, R is the reflection coefficient of PRS, Lr is the resonant length-distance between the ground plane and the PRS, λ is the operating wavelength, Δf is the difference between the high and low frequencies (range of frequencies over which the return loss is acceptable), f_0 is the operating frequency.

To examine the FPC operation condition, full-wave EM simulation using HFSS specifying periodic boundary conditions (PBCs) and Floquet ports to simulate the infinite periodic model of metamaterial superstrate has been done with simulated reflection coefficient (magnitude and phase) plotted in Fig. 3. It is obvious that the reflection phase (φ) of the proposed metasurface superstrate is 0 degrees and the reflection magnitude (p) is 0.65.

As per the geometrical optics model [16], the ground plane has a complex reflection coefficient superstrate has a complex reflection coefficient. The ground plane is a metallic conductor with a reflection phase close to π ($\varphi 1 \approx \pi$). The improvement in directivity [17] is given by (4) using the value of (p) from Fig. 3.

$$\Delta D(dB) = 10\log 10 \frac{1+p}{1-p} \tag{4}$$

Hence, ΔD is found out to be 6.7 dB using FEM. Theoretically, the refractive index (η) can be found as in (5).

$$\eta = \frac{Im\{\ln(e^{j2nk_o d})\} + 2m\pi - jRe\{\ln(e^{j2nkod})\}}{2k_o d} \tag{5}$$

where k_0 is the wavenumber in free space, d is HS, n is the integer. Putting values $\eta = 0.4$. The reflection coefficient is related to the

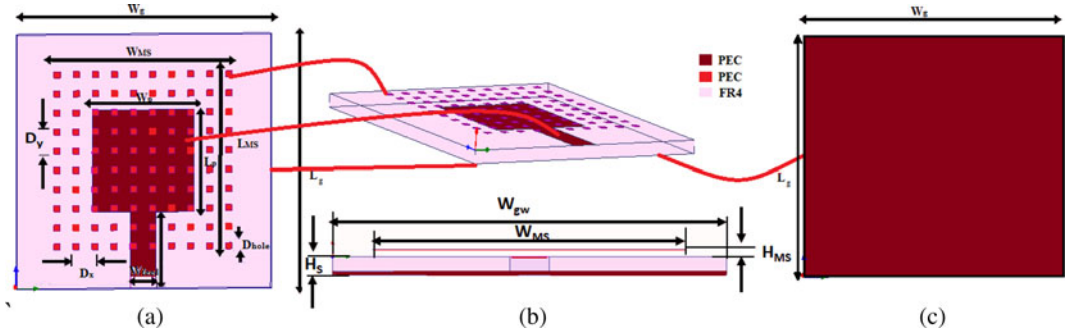

Fig. 1. Geometry of the metasurface antenna ($L_P = W_P = 16$ mm, $W_{feed} = 13.92$ mm $L_{feed} = 41.74$ mm, $L_{MS} = W_{MS} = 131$ mm, $L_g = W_g = 139$ mm, $D_X = D_y = 3.5$ mm, $D_{hole} = 3.5$ mm) (a) top view (b) side view (c) bottom view.

https://doi.org/10.1017/S1759078721001380 Published online by Cambridge University Press

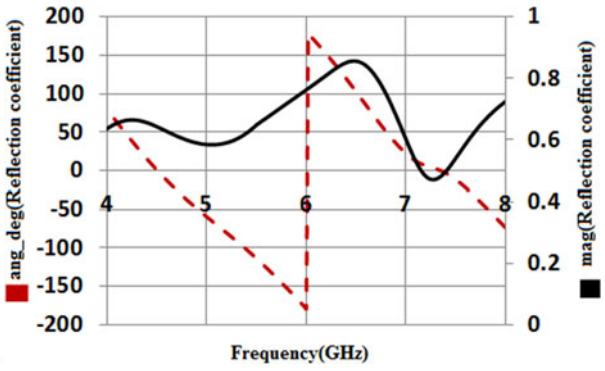

Fig. 3. Reflection phase and magnitude of proposed superstrate with Floquet port set-up for FEM Analysis.

refractive index by (6).

$$p = \frac{(1 - e^{(2k_o d)})\eta}{(1 - \eta^2 e^{(2k_o d)})} \tag{6}$$

Putting values $p = 0.67$ and using (4), the improvement in directivity comes out to be 7 dB.

Fabry–Perot cavity design results

The simulated reflection coefficients of the unloaded and metasurface superstrate loaded patch antenna are shown in Fig. 4. The unloaded patch antenna is resonating at 4.5 GHz with a reflection coefficient = 12 dB. When using the metasurface superstrate, strong resonance is generated in the cavity which enhances the matching over a wider band, covering the original frequency (4.5 GHz). The metasurface antenna is in a good matching with a maximum return loss = 23.5 dB, at the resonance frequencies 4.5 and 5 GHz. The bandwidth increases more than four times (4.25 to 4.75 GHz). The FPC antenna with periodic square cells has the maximum impedance matching bandwidth of 11% (in comparison to 2% of the patch antenna).

The fabricated antenna porotype is shown in Fig. 5. It is worth commenting that four pin screws of plastic material were used for the assembly of the antenna with superstrate on the top and ground plane on the bottom. A comparison between the reflection coefficient of the simulated and fabricated structures, shown in Fig. 5, is added to Fig. 4. The measurement was done using Keysight RF Fieldfox Network Analyzer. The comparison confirms that the measurement results agree with the simulated ones.

To validate the effect of the employed metasurface layers, different loading elements, shown in Fig. 6, as periodic square cells, periodic *S*-shaped cells, periodic Ω-shaped cells, periodic hole array [18–21] were examined. In objective of the designing reflective structure, the attention was focused on the directive gain improvement and bandwidth enhancement simultaneously. Many different periodic metamaterial elements such as square cell, *S*-shaped, Ω-shaped, hole element array, as shown in Fig. 6, have been considered. The PFC antenna loaded with these elements is as the metasurface layer were simulated and the simulated reflection curves are shown in Fig. 7. The periodic square cell elements were used which results in the best enhancement of the reflection coefficient. It has a maximum impedance matching bandwidth (−10 dB condition) of 22.2% in comparison to 8.89% of the patch antenna as calculated from equation 2.

Antenna radiation properties

The simulated directive-gain curves in XZ and YZ planes for the conventional patch antenna case and the metasurface superstrate loaded cases are plotted in (Figs 8(a) and 8(b)), respectively. As shown in Fig. 8(a), the peak directivity is 5 dB, and Front to back lobe ratio is 7 dB (5-(−2) dB). On the other hand, in Fig. 8(b), when the superstrate loads the antenna the peak directivity becomes 12 dB, and the front to back lobe ratio is 20 dB (12-(−8) dB). The enhancement in directivity agrees with the

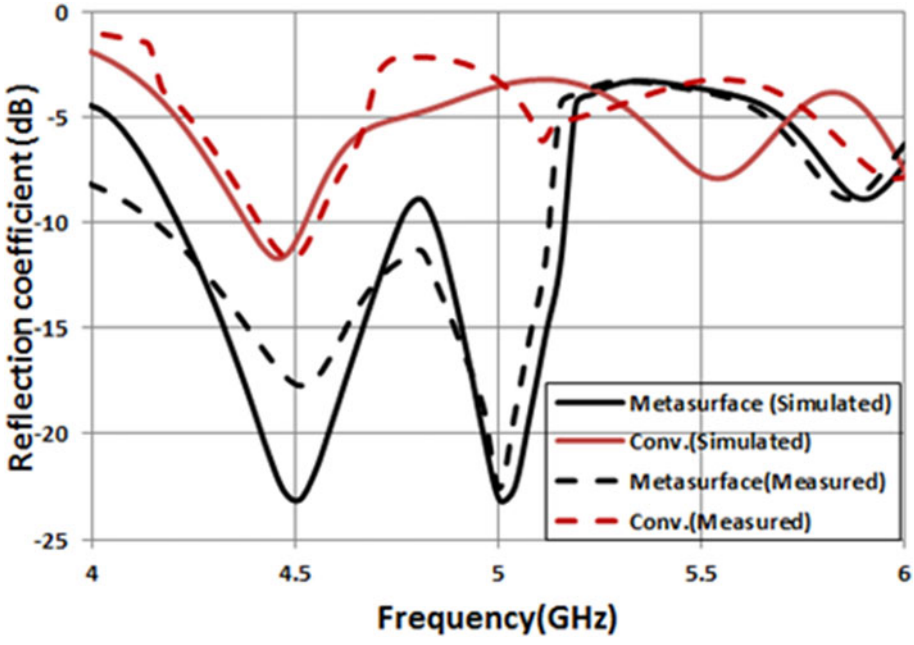

Fig. 4. Simulated reflection coefficient for the proposed antenna (without and with using metasurface substrate).

https://doi.org/10.1017/S1759078721001380 Published online by Cambridge University Press

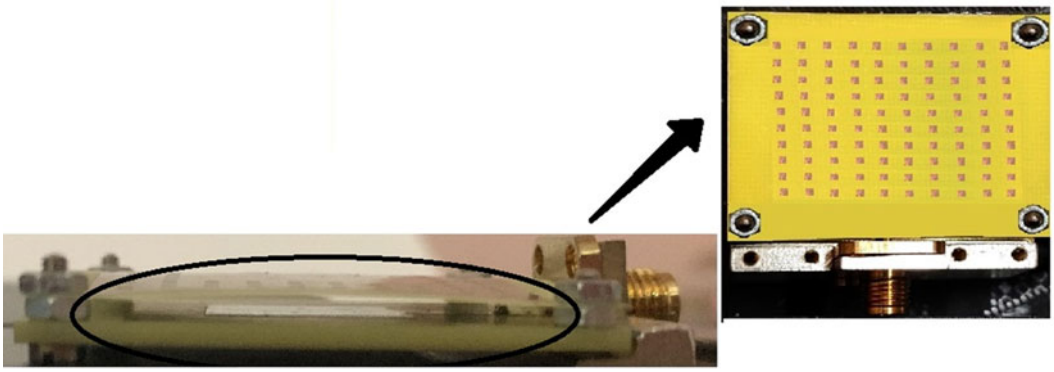

Fig. 5. Fabricated Fabry–Perot cavity antenna.

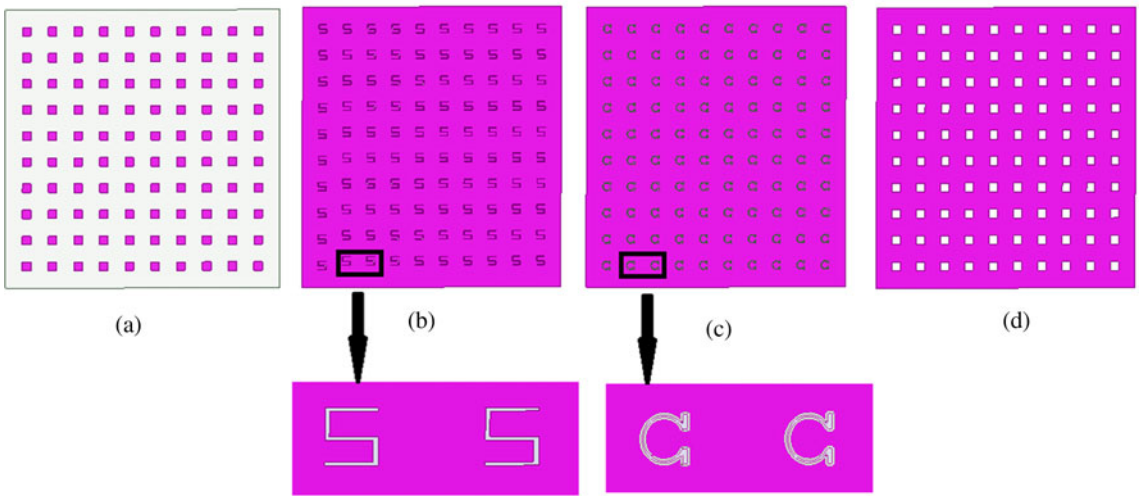

Fig. 6. Various reflective surfaces used as superstrate in the FPC antenna: (a) square cell, (b) *S*-element, (c) Ω-element (d) hole element.

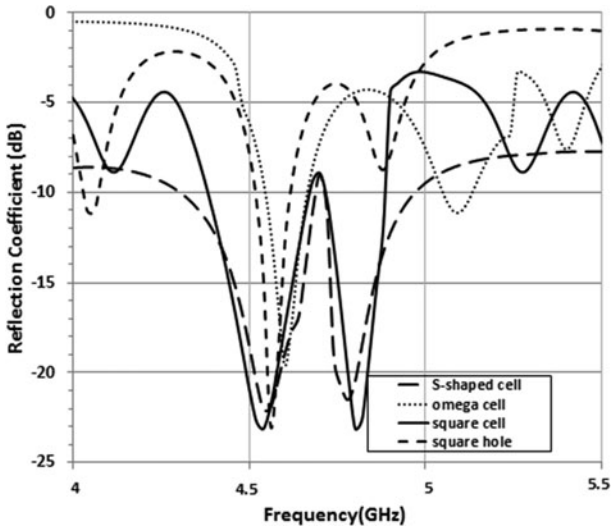

Fig. 7. Simulated reflection coefficient of the loaded patch antenna with *S*, Omega, patch, periodic holes cells.

previously shown theoretical results (improvement by 7 dB). This leads to a 140% improvement in directivity and 186% improvement in front-to-back lobe ratio along with its physical protection.

Using AMITEC gain measurement set-up as shown in Fig. 9(a). This setting was placed in an anechoic chamber shown in Fig. 9(b) where we manually had to take this gain measurement setup inside the chamber for measuring the radiation pattern.

In the setup given by AMITEC ['https://amitec.co/training/antenna-training-system-ats04/'], transmitted power is −40 dBm, received power is −78.92 dBm, transmitting antenna gain is 10 dB, and the distance between transmitting and receiving antenna is 2 m. Using these values and taking logarithm on both sides of Friis Equation, the antenna-gain values of receiving antenna is 3.63 dB and directivity is 12.2 dB. Therefore, a 2% error in the directivity of the fabricated antenna is obtained when compared with simulated. The errors can be accounted to fabrication tolerances or testing environment etc. The upward shift in boresight gain is mainly due to the tolerance of the dielectric constant of the FR4 substrate that is specified as 4.4 ± 5% [22].

https://doi.org/10.1017/S1759078721001380 Published online by Cambridge University Press

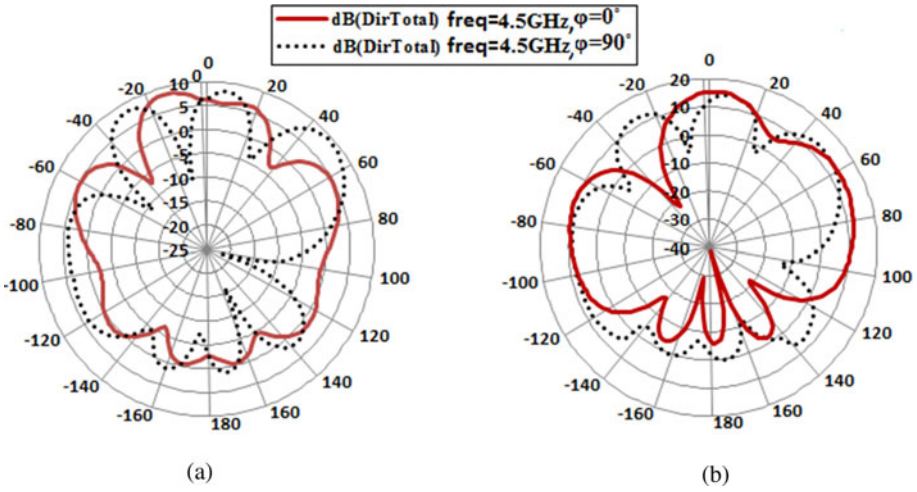

Fig. 8. Simulated directive pattern for the (a) single patch antenna, (b) proposed metasurface superstrate antenna in XZ and YZ planes.

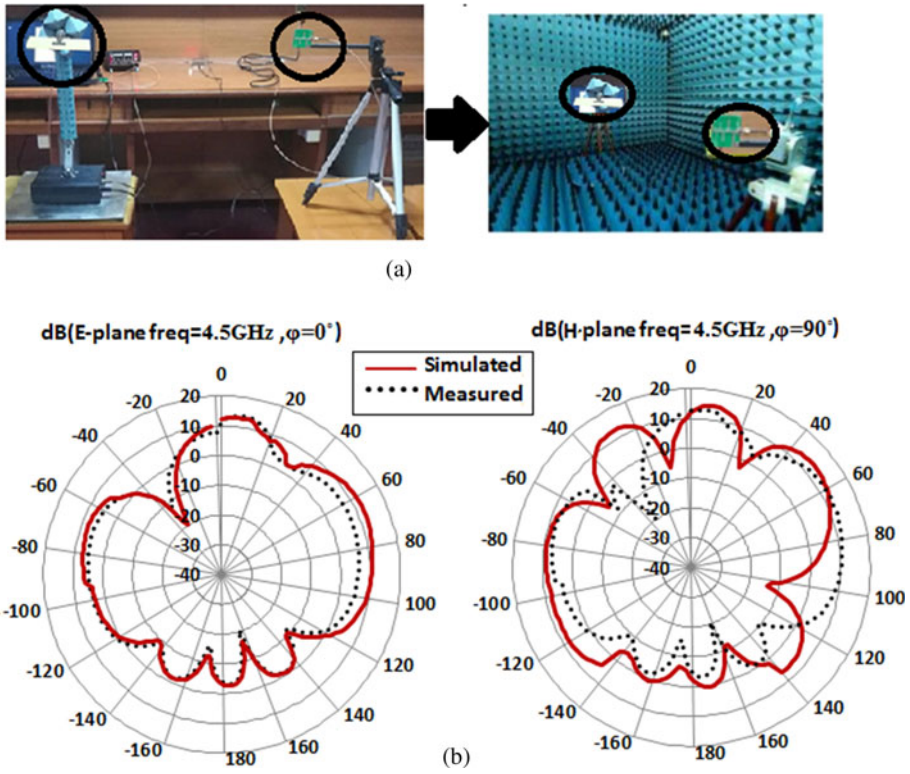

Fig. 9. (a) AMITEC gain measurement set-up (b) comparison of directivity (dB) at 4.5 GHz of simulated and fabricated metasurface antenna.

Toroidal patch antenna with superstrate

Toroidal metal structure design

It is seen in the previous section that the metasurfaces are capable of improving the bandwidth of the antenna but still not to a level that the antenna could be called broadband (the metasurface is somehow narrowband). This section proposes a toroidal metal structure with the capability of enhancing directivity and bandwidth simultaneously.

As mentioned earlier, the square and circle SRR are two basic metamaterial resonator shapes. In this section, a third basic metamaterial shape i.e. a triangle has been explored. The triangular single ring unit cell (a toroidal metal structure) is shown in Fig. 10. The cell has been designed in such a way that its outer perimeter is the same as that of the circular SRR ($r_{ext} = 6.9$ mm). The advantage of using a triangle shape is a better degree of control as it has more variable parameters than a circle or square shape, i.e. length, breadth, height, and angle between two arms.

The equivalent circuit of the Toroidal metal structure is shown in Fig. 11. The values of $C_{eq} = 70\ C_{pul}$ (i.e. capacitance per unit length) and $LT = 1.59 \times 10^{-8}$ H are obtained using the same formula as for square SRR [23]. The average length is calculated to be $l_{avg} = 35.4$ mm; thus, $C_{eq} = 1.03 \times 10^{-9}$ F. The value of resonant frequency is found out to be 3.93 GHz and for circular-shaped SRR is 4.53 GHz i.e. more than triangular SRR. Therefore, it is observed that the filling ratio i.e. (a/λ) of triangular SRR is more than circular SRR. Hence, it is a better candidate for metamaterial than a circular SRR.

The advantage of the toroidal cell is it has a high magnetic field as a consequence of toroidal currents in its anti-symmetric arms. Toroidal functionality can be explained by simulating a

https://doi.org/10.1017/S1759078721001380 Published online by Cambridge University Press

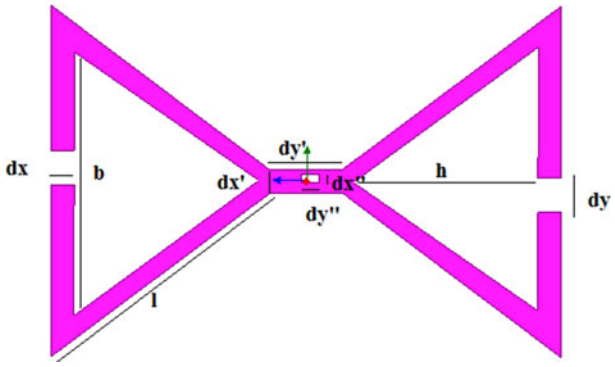

Fig. 10. Toroidal metal structure with dimensions dx = 0.5 mm, dy = 1 mm, dx" = 0.5 mm, dy" = 1.3 mm, dx" = 0.15 mm, dy" = 0.3 mm, l = 4.8 mm, b = 4.3 mm, h = 3.5 mm.

2-port unit cell of meta-molecule Fig. 12(a) illustrates the magnetic field intensity distribution in a plane perpendicular to the array and Fig. 12(b) illustrates the surface current distribution forming toroidal moment because of their anti-symmetric flow in both arms. The circular loop current excited on the XY plane of the metasurface creates a magnetic moment on it. Thus, this leads to a toroidal moment oscillating back and forth along the axis of the metal molecule. The two side gaps also support a magnetic quadrupole moment. It is seen that the resonant magnetic fields at the center of two consecutive elements are in phase.

Mathematical analysis

Considering metasurface superstrate patch antenna loaded with toroidal metal structures, the field reaching the observer plane

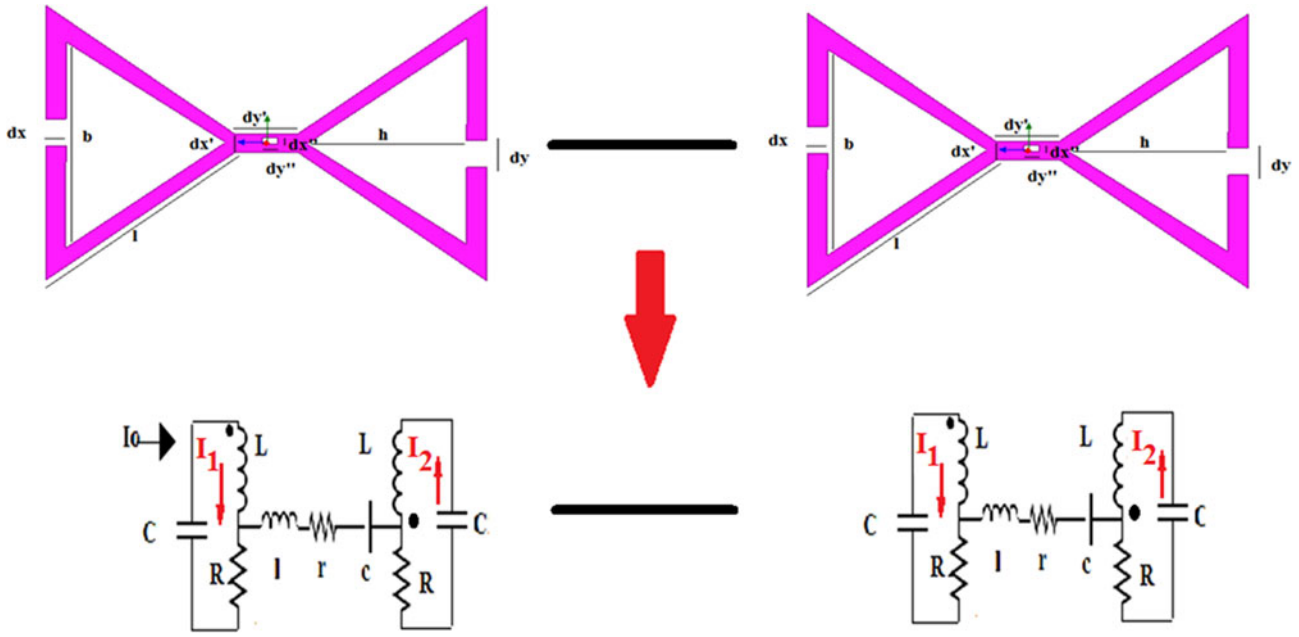

Fig. 11. Equivalent circuit model of toroidal metal structure.

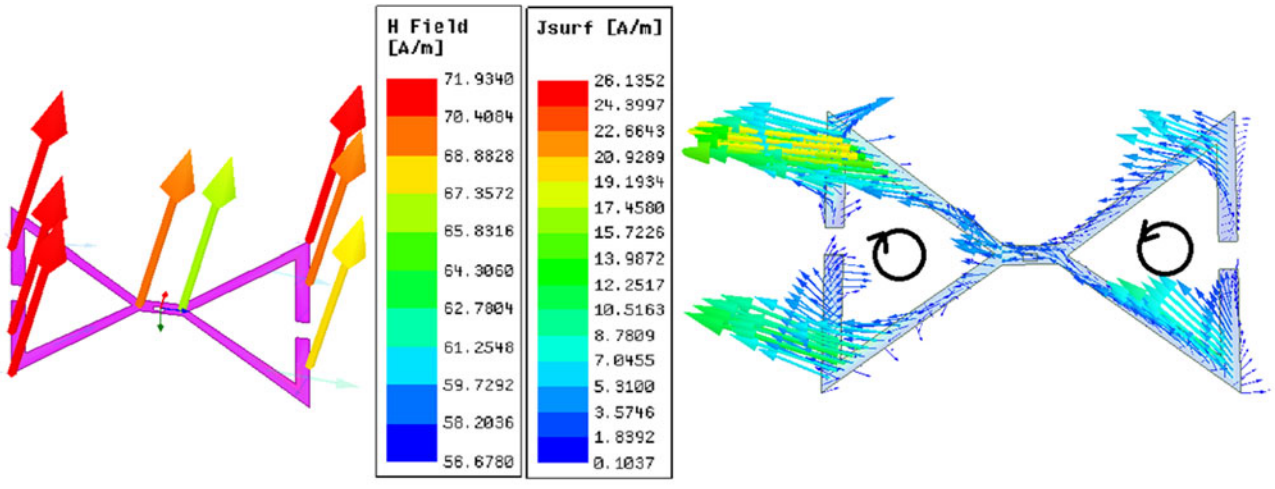

Fig. 12. Simulated distribution plot of toroidal metal structure for (a) magnetic field (b) surface current.

https://doi.org/10.1017/S1759078721001380 Published online by Cambridge University Press

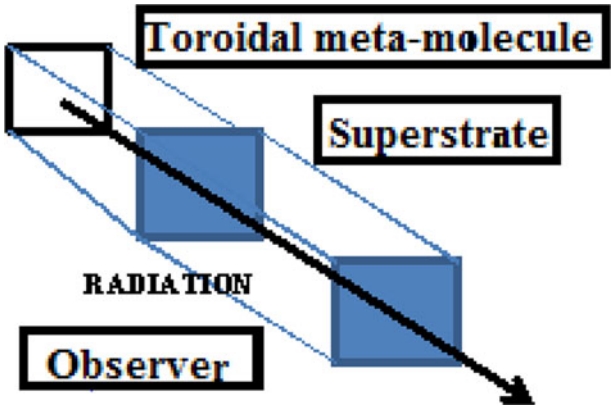

Fig. 13. Plane setup for measurement of radiation at observer plane.

(OP) can be found by Fourier propagating the field distribution at the intermediate superstrate up to the OP as shown in Fig. 13.

The total field (E) radiated by a 2×2 planar array of toroidal meta-atoms is obtained by summing the contributions from all at the position of the observer is given by (7).

$$E = \sum_r E(r) \approx \frac{1}{\Delta^2} \int_{array} d^2 r E(r) \tag{7}$$

Equation (7) holds provided that all meta-atoms oscillate in phase and that the separation between meta-atoms is sufficiently smaller than the wavelength of incident radiation. The latter assumption replaces the sum over the unit cells with an integral over the array area (Δ^2). In Fig. 13, three planes have been introduced: the array plane, the superstrate plane (SP), and OP [24–26]. $Y_{l,l'',m}$ are the spherical vector harmonics that represent any vector field on the surface of the unit sphere in the same way as spherical harmonics represent any scalar field on the surface of the unit sphere.

The current is given by (8).

$$I_{l,m} = \int_0^{2\pi} d\varphi' \int_0^{\infty} \rho . d\rho . Y_{l,m}\ (\theta, \varphi' + \pi)\ \frac{\exp(-ikr)}{r} \tag{8}$$

where ρ and φ" are the radius and the angle specifying the position of toroidal meta-atoms, r is the distance between the observer and toroidal meta-atom, θ is the angle between the line connecting the observer to a toroidal meta-atom and its normal, and R is the distance from the observer to the toroidal array.

The directivity of the antenna is given by (9).

$$D(\theta, \varphi) = \frac{4\pi U(\theta, \varphi)}{P_{rad}} \tag{9}$$

where $U\ (\theta, \varphi)$ represents normalized radiation pattern and is given by (10).

$$U(\theta, \varphi) = \frac{r^2}{2\eta} |E_\varphi^2 + E_\theta^2| \tag{10}$$

Therefore, to calculate directivity, the equivalent circuit model [27] can be used to determine the ratio of the total currents using the equivalent circuit, shown earlier in Fig. 11. In the equivalent circuit, the current entering the toroidal meta-atom is assumed to be Io, and I1 and I2 are the anti-symmetric currents in the triangular SRR. The segment joining the two triangular split rings plays a role in altering the direction of the current. However, its R, L, C can be considered negligible. The current and voltages in each meta-atom can be found out from (11) and (12) where V_1 is the voltage at the input terminal and V_2 is the voltage at the output terminal of corresponding rings in meta-atom.

$$V1 = -\frac{1}{j\omega} . \frac{(I_0 - I_1)}{C} = (R - j\omega L)\ I1 \tag{11}$$

$$V_2 = -\frac{1}{j\omega} \cdot \frac{I_2}{C} = -(R - j\omega L) I_2 \tag{12}$$

Using (11) and (12), the ratio of currents can be found out as in (13)

$$\frac{I_1}{I_o} = -\frac{-j\omega C(R - j\omega L)}{X(\omega)} \tag{13a}$$

$$\frac{I_2}{I_o} = -\frac{-j\omega(-j\omega L)}{X(\omega)} \tag{13b}$$

$$X(\omega) = -\omega^3 C^2 [-L^2\omega - 2jRL] + \omega^2[(R^2 - C^2) - 2CL] - 2j\omega RC + 1 \tag{13c}$$

A linear array of meta-atoms separated by distance "d" radiating in end-fire direction is formed as shown in Fig. 11 with excitation coefficients as $I_o = 1$, $I_o' = \pm e^{jkd}$ and $d = 0.1\ \lambda$. The directivity given by (14) was obtained by putting optimal excitation coefficients for currents [28] and then doing Taylor series expansion of ratio of excitation coefficients assuming $kd << 1$.

$$D = I_{1optimal} + I_{2optimal} + ee^{\pm kd} \tag{14a}$$

$$\left[\frac{I_1}{I_2}\right] = optimal = \frac{1 - \frac{3}{2} pe^{\pm jkd}}{e^{\pm jkd} - \frac{3}{2} p} \tag{14b}$$

$$p = \frac{sin(kd)}{kd}\left[1 - \frac{1}{(kd)^2}\right] + \frac{cos(kd)}{(kd)^2} \tag{14c}$$

Using the set of equations (14a)– 14c), $D_{\text{optimal}} \approx 28.57$ or 14.5 dB

Energy harvesting applications

A parallel plate system is formed between a plane containing a toroid and a plane containing a superstrate. This is proposed capacitive energy harvester system, where the curling magnetic field density (B) accelerated by toroidal meta-atoms produces the changing electric field (E) as elucidated by Maxwell's equation [29] as in (15)

$$\nabla XB = \mu_0 \varepsilon_0 \frac{\partial E}{\partial t} \tag{15}$$

https://doi.org/10.1017/S1759078721001380 Published online by Cambridge University Press

where μ_0 is the magnetic permeability and ε_0 is the electric permittivity of free space between the two annular plates. The toroid meta-atoms are spaced at r_1 and r_2 from the patch feed point. The curl can now be written as

$$\nabla XB = -\frac{\mu_0 I}{4\pi}\frac{\partial E}{\partial t}\frac{1}{r}\left[\frac{\partial}{\partial r}\left(\int_{r_1}^{r_2}\frac{1}{r}\partial r\right)\right]\hat{z} \tag{16}$$

Then by substituting (16) into (15), a model of changing electric field is obtained as

$$\frac{\partial E}{\partial t} = \frac{-\mu I}{8\pi\mu_0\varepsilon_o}\left[\frac{1}{r_2^2}-\frac{1}{r_1^2}\right]\hat{z} \tag{17}$$

Assuming the time-varying current is to be alternating as a sinusoidal function of time and angular frequency (ω), the electric field between the superstrate and patch plane varying with time comes out to be

$$E = \frac{-\mu I}{8\pi\mu_0\varepsilon_o}\left[\frac{1}{r_2^2}-\frac{1}{r_1^2}\right]I_o\omega cos(\omega t)\hat{z} \tag{18}$$

From (18), the induced voltage for capacitive energy harvester is obtained as

$$V = \frac{E}{d} = E = \frac{-\mu I}{8\pi H_{MS}\mu_0\varepsilon_o}\left[\frac{1}{r_2^2}-\frac{1}{r_1^2}\right]I_o\omega\cos(\omega t)\hat{z} \tag{19}$$

Thus, it can be observed that the proposed capacitive energy harvester is a function of the gap "H_{MS}" between the plates i.e. the patch plane and SP.

Simulated results

The comparison of simulation of the toroidal metasurface antenna's directivity of a patch antenna with and without toroid is shown in Fig. 14. The patch with toroidal metal structure and superstrate directivity is 15 dB. There is a slight error between the theoretical and simulated values.

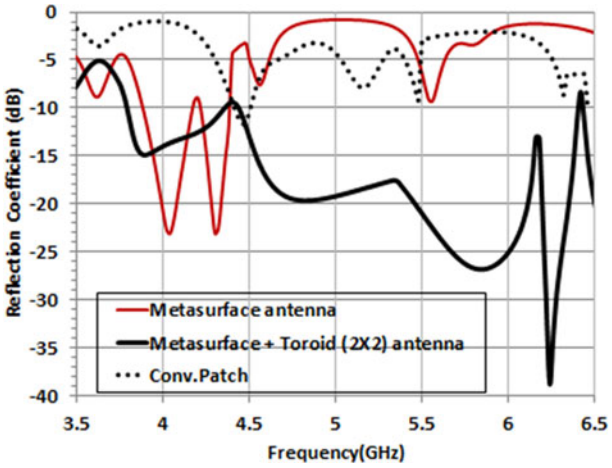

Fig. 15. Comparison of bandwidth at 4.5 GHz of simulated metasurface antenna with toroid /without toroid vs conventional antenna.

The comparison of simulation reflection coefficient curves of a toroidal metasurface antenna with a conventional patch antenna and without toroid is shown in Fig. 15. The 10 dB impedance bandwidth obtained through simulation of the patch with toroidal metal structure and superstrate is 34%. Therefore, the bandwidth increases eight times using the proposed structure comparing with the conventional patch. It can be claimed that this state-of-art improves the bandwidth by 800% and directivity by 200% which is the first-ever proposed in the literature, using a single layer of the metasurface.

Simulated Current Distribution

The simulated current distribution at 4.5 GHz is shown in Fig. 16 (a) for a single microstrip patch and Fig. 16(b) for the metasurface-loaded patch antenna. When the Fourier transform of a short pulse is taken, a broad frequency spectrum is obtained. This analogy is used in determining the radiation pattern of an antenna: the pattern can be thought of as the Fourier transform

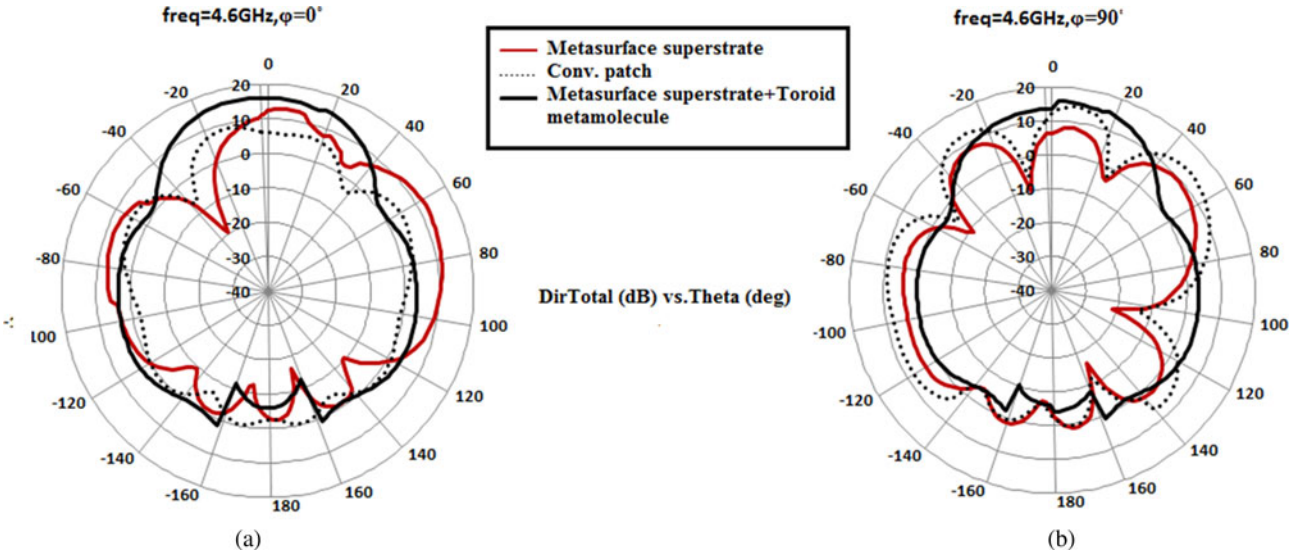

Fig. 14. Comparison of directive gain (dB) at 4.5 GHz of simulated metasurface antenna with toroid /without toroid vs conventional antenna.

https://doi.org/10.1017/S1759078721001380 Published online by Cambridge University Press

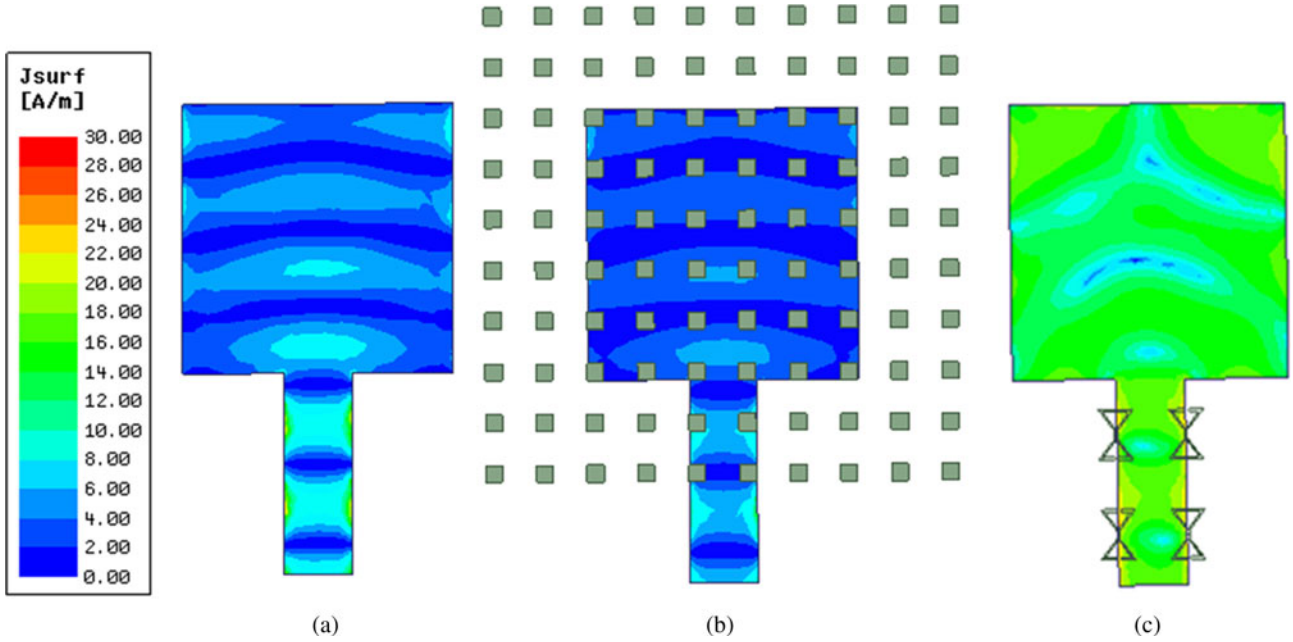

Fig. 16. Simulated current distribution plot of (a) conventional patch antenna (b) metasurface superstrate antenna (c) antenna with proposed toroidal metal structure and superstrate.

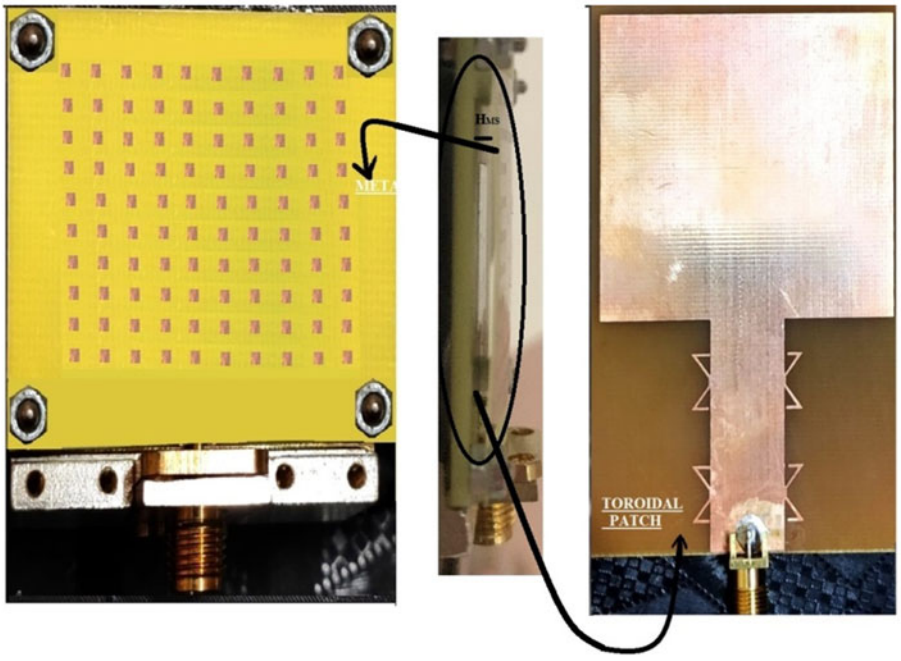

Fig. 17. Fabricated toroid metasurface superstrate antenna.

of the antenna's current or voltage distribution [30]. As a result, small antennas have broad radiation patterns (low directivity), and antennas with large uniform voltage or current distributions have very directional patterns (and thus, a high directivity) as evident from Fig. 16(b). This further confirms the directivity enhancement.

The patch antenna is further loaded with four toroidal metal structures at areas where current density was comparatively higher (as shown in Fig. 16(b). As a consequence, the current distribution is more uniform and higher on the patch as seen in Fig. 16(c). There is a 38% increase in current density i.e. from 5 to 24 A/m on the patch.

Fabrication measured results

The fabricated prototype of the metasurface superstrate toroid antenna is shown in Fig. 17. The antenna performance was evaluated by checking its matching properties and EM radiation properties as shown in Fig. 18 by plotting the simulated and measured reflection coefficient. It is obvious that the results agree with each

https://doi.org/10.1017/S1759078721001380 Published online by Cambridge University Press

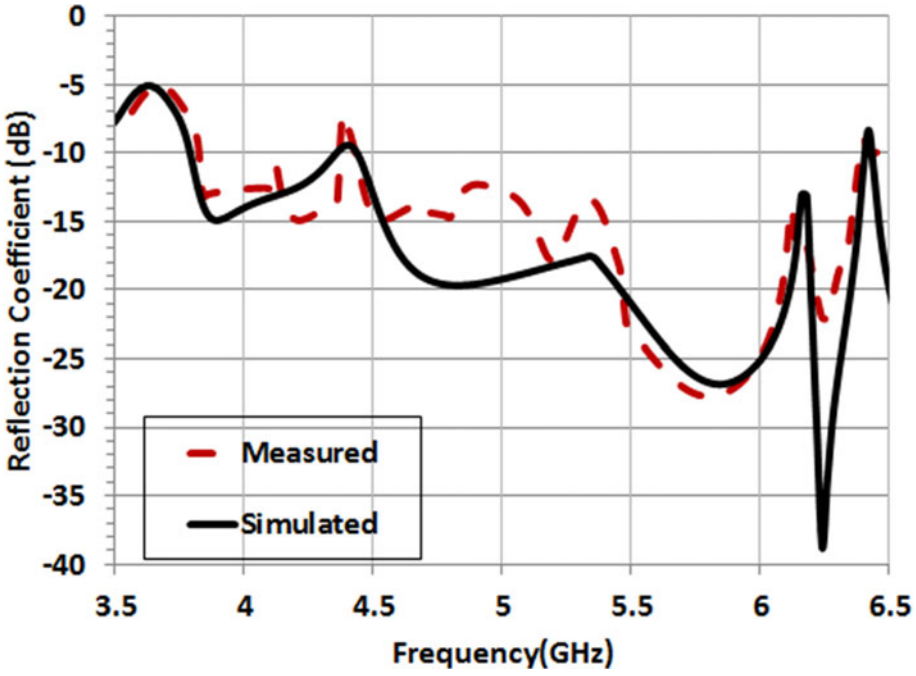

Fig. 18. Comparison of reflection coefficient at 4.5 GHz of simulated metasurface antenna with toroid vs fabricated antenna.

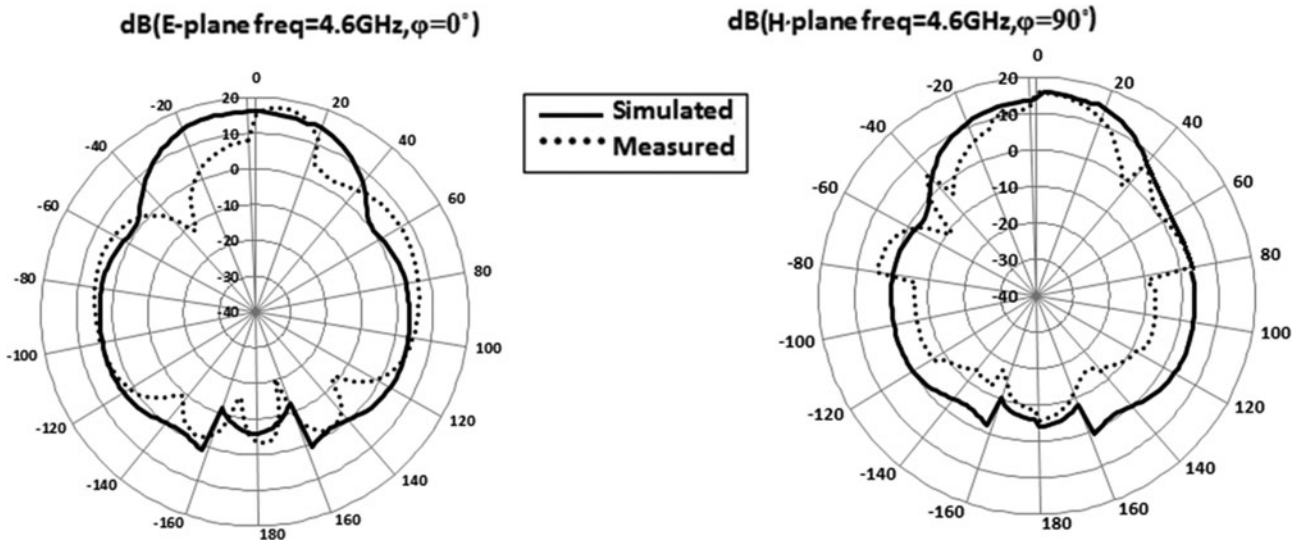

Fig. 19. Comparison of directive gain (dB) at 4.6 GHz of simulated metasurface antenna with toroid vs fabricated antenna.

other and also both of them are lower than – 10 dB from almost 3.7 to 4.4 GHz and 4.42 GHz to near 6.5 GHz.

A comparison between simulated and measured antenna radiation patterns and reflection curves at 4.5 GHz is shown in Fig. 19. The results are close to each other. As shown in Fig. 19(a), the peak directivity is 15 dB, and Front to back lobe ratio is 20 dB (15-(−5) dB). The enhancement in directivity agrees with the previously shown theoretical results. This leads to a 200% improvement in directivity and 800% improvement in bandwidth with a 20 dB front-to-back lobe ratio along with its physical protection.

Using AMITEC gain measurement set-up as shown in Fig. 9(a), the radiation pattern was measured and plotted in Fig. 19(a). In the setup given by AMITEC, transmitted power is −40 dBm, received power is −75.09 dBm, transmitting antenna gain is 10 dB, and the distance between transmitting and receiving antenna is 2 m. Using these values and taking logarithm on both sides of Friis Equation, the antenna-gain values of receiving antenna is 6.6 dB and directivity is 15.2 dB. Therefore, a 2% error in the directivity of the fabricated antenna is obtained when compared with the simulated (shown in Fig. 14). The discrepancy between the simulated and measured results for reflection coefficient as shown in Fig. 19(b), the difference in peaks can be accounted to the tolerance of the dielectric constant of the FR4 substrate that is specified as 4.4 ± 5% [26] and to fabrication tolerances or testing environment, etc. However, the 10 dB bandwidth is measured the same as the simulated one.

Finally, a comparison of the proposed antenna with existing state of art antenna structures [27–31] using FPC has listed in Table 1. All the reference antennas have larger dimensions except [31, 32]. The bandwidth of the proposed antennas is significantly

https://doi.org/10.1017/S1759078721001380 Published online by Cambridge University Press

Table 1. Comparison of proposed work with reference antennas.

Ref.	10 dB impedance BW (%)	Front/back ratio (dB)	Maximum directivity (dB)	Antenna size
[27]	11.6	20	17.4	$2.83\,\lambda_0 \times 3.23\,\lambda_0 \times 0.49\,\lambda_0$
[29]	2.6	21	17.3	$5\,\lambda_0 \times 5\,\lambda_0 \times 0.5\,\lambda_0$
[30]	Not reported	16	16.3	$2.21\,\lambda_0 \times 2.21\,\lambda_0 \times 578\,\lambda_0$
[31]	30	14	14.2	$1.6\,\lambda_0 \times 1.6\,\lambda_0 \times 0.84\,\lambda_0$
[32]	14.7	Not reported	10.5	$2\,\lambda_0 \times 2\,\lambda_0 \times 0.77\,\lambda_0$
[33]	22	Not reported	Decreases by 6.5 dB	$2.65\,\lambda_0 \times 2.65\,\lambda_0 \times 0.86\,\lambda_0$
[34]	32	Not reported	Decreases by 2.5 dB	$1.9\,\lambda_0 \times 1.87\,\lambda_0 \times 1.77\,\lambda_0$
Our Work	34	20	15	$2.13\,\lambda_0 \times 2.13\,\lambda_0 \times 0.25\,\lambda_0$

more than the reference antennas. In [33, 34], the antennas are wideband as they use superstrate but this has led to a decrement in the directivity of the antenna. Also, in [27, 29], the antennas have high directivity at the expense of decreasing the antenna bandwidth. It is noticeable that the proposed antenna has the highest front-to-back lobe ratio. Therefore, it can be claimed that the proposed antenna which is designed using just a single layer of superstrate improves the antenna directivity and bandwidth simultaneously and has a compact size and lower height in comparison with the reported antennas.

Conclusion

A new wideband and directive toroidal metasurface antenna is designed and analyzed using a substrate with $\varepsilon r = 4.4$. Antenna performance parameters, especially reflection co-efficient and front-to-back lobe ratio, enhanced. The antenna covers a complete band from 4.2 to 8 GHz. It becomes well isolated and protected from the outside environment with 200% enhancement in directivity (10 dB directivity enhancement), 186% increase in front to back lobe ratio, 8 times improvement in bandwidth compared to conventional unloaded patch antenna. This idea is demonstrated for the first time for the best to authors' knowledge.

References

1. **Lajevardi M and Kamyab M** (2017) Ultraminiaturized metamaterial-inspired SIW textile antenna for off-body applications. *IEEE Antennas and Wireless Propagation Letters* **16**, 3155–3158.
2. **Sharma SK, Abdalla MA and Chaudhary RK** (2017) An electrically small SICRR metamaterial`-inspired dual-band antenna for WLAN and WiMAX applications. *Microwave and Optical Technology Letters* **59**, 573–578.
3. **Singh H, Sohi BS and Gupta A** (2021) Designing and performance evaluation of metamaterial inspired antenna for 4 G and 5 G applications. *International Journal of Electronics* **108**, 1035–1057.
4. **Kanth VK and Raghavan S** (2020) Ultrathin wideband slot and patch FSS elements with sharp band edge characteristics. *International Journal of Electronics* **107**, 1365–1385.
5. **Trentini GV** (1956) Partially reflecting sheet arrays. *IRE Transactions on Antennas and Propagation* **4**, 666–671.
6. **Chacko PB, Augustin G and Denidni TA** (2016) FPC Antennas: c-band point-to-point communication systems. *IEEE Antennas and Propagation Magazine* **58**, 56–64.
7. **Holloway LC, Kuester EF, Gordon JA, O'Hara J, Booth J and Smith DR** (2012) An overview of the theory and applications of metasurfaces: the two-dimensional equivalents of metamaterials. *IEEE Antennas and Propagation Magazine* **54**, 10–35.
8. **Wang J, Li Y, Jiang ZH, Shi T, Tang MC, Zhi Ning Chen ZZ and Qiu CW** (2020) Metantenna: when metasurface meets antenna again. *IEEE Transactions on Antennas and Propagation* **68**, 1332–1347.
9. **Xiang H, Ge L, Liu L, Jiang T, Zhang ZQ, Chan CT and Han D** (2017) A generic minimal discrete model for toroidal moments and Iits experimental realization. *Physical Review B* **95**, 045403.
10. **Fedotov VA, Rogacheva AV, Savinov V, Tsai DP and Zheludev NI** (2013) Resonant transparency and non-trivial non-radiating excitations in toroidal metamaterials. *Scientific Reports* **3**, 2967.
11. **Miroshnichenko AE** (2015) Nonradiating anapole modes in dielectric nanoparticles. *Nature Communications* **6**, 8069.
12. **Wu MF, Meng FY and Wu Q** (2005) A compact equivalent circuit model for the SRR structure in metamaterials. *Asia-Pacific Microwave Conference Proceedings* **1**, 1–4.
13. **Lee YJ, Yeo J, Mittra R and Park WS** (2005) Thin Frequency Selective Surface (FSS) superstrate with different periodicities for dual-band directivity enhancement. Proceedings of the IEEE International Workshop on Antenna Technology: Small Antennas and Novel Metamaterials (IWAT '05), pp. 375–378.
14. **Ji L, Fu G and Gong S-X** (2016) Array-Fed beam-scanning partially reflective surface (PRS) antenna. *Progress in Electromagnetics Research Letters* **58**, 73–79.
15. **Liu A, Lei S, Shi X and Li L** (2013) Study of antenna superstrates using metamaterials for directivity enhancement based on Fabry–Perot resonant cavity. *International Journal of Antennas and Propagation*, **2013**, 1–10.
16. **Razi ZM, Bahadori N and Rezaei P** (2013) A comparative study on the directivity enhancement of the Patch, SRR and Omega unit cells as Fabry–Perot superstrate. 2nd Asian symposium on electromagnetics and photonics engineering, pp. 147–148.
17. **Razi ZM, Rezaei PR and Bahadori N** (2013) Directivity improvement of microstrip antenna with S metamaterial unit cell as Fabry–Perot cavity superstrate. 2nd Asian symposium on electromagnetics and photonics engineering, pp. 127–128.
18. **Razi ZM and Rezaei P** (2013) Design and simulation of directivity microstrip patch antenna by Fabry–Perot Omega unit cells. *IEEE APS International Symposium on Antennas and Propagation*, pp. 762–763.
19. **Microwave Journal e-book** (2018) Selection of PCB materials for 5G. *Rogers Corporation*, p. 3.
20. **Bilotti F, Toscano A, Vegni L, Aydin K, Alici KB and Ozbay E** (2007) Equivalent-circuit models for the design of metamaterials based on artificial magnetic inclusions. *IEEE Transactions on Microwave Theory and Techniques* **55**, 2865–2873.
21. **Rydström S and Lindhe O** (2006) Efficient calculations of antenna radiation patterns using the fast Fourier transform. *AIP Conference Proceedings* **7**, 834.
22. **Dubovik VM and Cheshkov AA** (1975) Multipole expansion in classical and quantum field theory and radiation. *Soviet Journal of Particles and Nuclei* **5**, 318.
23. **Radescu EE and Vaman G** (2002) Exact calculation of the angular momentum loss, recoil force, and radiation intensity for an arbitrary source in terms of electric, magnetic, and toroid multipoles. *Physical Review E* **65**, 046609.
24. **Tatartschuk E, Gneiding N, Hesmer F, Radkovskaya A and Shamonina E** (2012) Mapping inter-element coupling in metamaterials: scaling down to infrared. *Journal of Applied Physics* **111**, 094904.
25. **Griffiths DJ** (1999) *Introduction to Electrodynamics*, 3rd Edn. New Jersey, NJ, USA: Prentice-Hall.
26. **Altshuler EE, O'Donnell TH and Yaghjian AD** (2005) A monopole super directive array. *IEEE Transactions on Antennas & Propagation* **53**, 2653–2661.
27. **Jagtap SD, Gupta RK, Chaskar N, Kharche SU and Thakare R** (2018) Gain and bandwidth enhancement of circularly polarized MSA using PRS and AMC layers. *Progress In Electromagnetics Research* **87**, 107–118.

https://doi.org/10.1017/S1759078721001380 Published online by Cambridge University Press

28. **Feresidis AP and Vardaxoglou JC** (2001) High gain planar antenna using optimized partially reflective surfaces. *IEEE Proceedings of Microwave & Antennas Propagation*, 345–350.
29. **Vaidya AR, Gupta RK, Mishra SK and Mukherjee J** (2014) Right-hand/left-hand circularly polarized high-gain antennas using partially reflective surfaces. *IEEE Antennas and Wireless Propagation Letters* **13**, 431–434.
30. **Singh AK, Abegaonkar MP and Koul SK** (2017) High-gain and high-aperture-efficiency cavity resonator antenna using metamaterial superstrate. *IEEE Antennas and Wireless Propagation Letters* **16**, 2388–2391.
31. **Chacko BP, Augustin G and Denidni TA** (2014) FPC Antennas, C-band, point to point communication. *IEEE Antennas and Propagation Magazine* **62**, 19–26.
32. **Vaid S and Mittal A** (2017) Wideband orthogonally polarized resonant cavity antenna with dual layer Jerusalem cross partially reactive surface. *Progress In Electromagnetics Research C* **72**, 105–113.
33. **Oliner AA** (2002) A periodic-structure negative-refractive-index medium without resonant elements. *IEEE-APS URSI International Symposium* **41**, 105–113.
34. **Monsoriu JA, Depine RA and Silvestre E** (2007) Non-Bragg band gaps in 1D metamaterial aperiodic multilayers. *Journal of European Optical Society Rapid Publication* **2**, 191–194.

Parul Dawar obtained B.Tech. in electronics and communication engineering from Guru Gobind Singh Indraprastha University (GGSIPU), Delhi, India in 2005. She completed her M.E. from Department of Electronic Science, Delhi University, India in 2007. She obtained the PhD degree from Delhi Technological University, India in 2018 and was awarded "Outstanding PhD Thesis Award" for the same in 2019. She had various internships during her bachelor's and master's in various laboratories of the Defense Research Development Organization, India. She is an assistant professor in the Electronic Engineering Department, Guru Tegh Bahadur Institute of Technology. She has published more than 20 peer-reviewed journal and conference papers. Her research interests are miniaturized, multiband and wideband microwave/millimeter antennas, metasurfaces, MESFET characterization, and ferrite fabrication. She is a member of the IEEE/URSI Commission B. She has authored two books on electromagnetic theory for B.Tech students designed as per curriculum of GGSIPU and Uttar Pradesh Technical University, India. She is open educational resources instructor at Progia Learnware for optical communication and has also reviewed papers in peer-reviewed journals and conferences.

Dr. Mahmoud A. Abdalla was born in 1973. He obtained B.Sc. and M.Sc. in electrical engineering from the Electrical Engineering Department, Military Technical College, Cairo, Egypt in 1995 and 2000. He obtained PhD from School of Electrical Engineering, University of Manchester, UK, in 2009. He is currently a professor and leads the electromagnetic waves group in the Electronic Engineering Department, Military Technical College. Dr. Mahmoud was the recipient of Egyptian encouragement state prize for engineering sciences in 2014. He has published more than 210 peer-reviewed journal and conference papers. His research interests are miniaturized, multiband wideband microwave/ millimeter antennas, components and absorbing materials with great attention to employ metamaterial/EBG structures. Dr. Mahmoud Abdalla is an IEEE senior member and European Microwave Association EuMA. He is currently a reviewer in many high-ranked electromagnetic journals. In 2018 and 2019, he was awarded as top 1% world reviewer as published by Publon. In 2020, he was named in the top 2% scientists in "A standardized citation metrics author database annotated for scientific field" and "Updated science-wide author databases of standardized citation indicators."

https://doi.org/10.1017/S1759078721001380 Published online by Cambridge University Press